

# High-fidelity large eddy simulation of combustion for propulsion and power

J. C. Oefelein<sup>1</sup> and R. Sankaran<sup>2</sup>

<sup>1</sup>Combustion Research Facility, Sandia National Laboratories, Livermore, CA 94551

<sup>2</sup>National Center for Computational Sciences, Oak Ridge National Laboratory, Oak Ridge, TN 37831

E-mail: oefelei@sandia.gov

**Abstract.** Development and application of the large eddy simulation (LES) technique for analysis of turbulent combustion and the related thermophysical flow processes in next-generation propulsion and power systems are widely recognized as a viable method for both science and engineering. Application of LES provides the formal ability to treat the full range of multidimensional time and length scales that exist in turbulent reacting flows in a computationally feasible manner and thus provides a way to simulate reacting flow phenomena in complex geometries at device relevant (i.e., high-pressure, high-Reynolds number) conditions. Here we provide a perspective on high-fidelity LES and its role in the development of predictive models. Emphasis is placed on processes typically encountered in state-of-the-art systems such as internal-combustion engines, gas turbines, and liquid rockets. These processes include highly nonlinear broadband transients, turbulence-chemistry interactions, and acoustic instabilities, all of which can have a profound effect on the operational characteristics of a given system.

## 1. Introduction

Turbulent multiphase combustion processes are prevalent in a wide variety of propulsion and power systems, including internal-combustion engines, gas turbines, and liquid rockets. As such, development of predictive models that reliably treat these processes is recognized as an important priority in research, and a variety of challenges arises. Turbulent flows involving heterogeneous chemically reacting and/or multiphase mixtures (as is the case for all propulsion and power devices) have a variety of complicating factors including highly nonlinear chemical kinetics, small-scale velocity and scalar mixing, turbulence-chemistry interactions, compressibility effects (volumetric changes induced by changes in pressure), and variable inertia effects (volumetric changes induced by variable composition or heat addition). Coupling between processes occurs over a wide range of time and length scales, many being smaller than can be resolved in a numerically feasible manner. Further complications arise when multiple phases are present because of the introduction of dynamically evolving interface boundaries and the complex exchange processes that occur as a consequence. At the device level, high-performance, dynamic stability, low pollutant emissions, and low soot formation must be achieved simultaneously in highly confined geometries that generate extremely complex flow and acoustic patterns. Flow and combustion processes are highly turbulent (i.e., integral-scale Reynolds numbers of  $\mathcal{O}(10^5)$  or greater), and turbulence dynamics are dominated by geometry and various operating transients. In many cases operating pressures approach or exceed the thermodynamic critical pressure of the fuel or oxidizer. Operation at elevated pressures significantly increases system Reynolds numbers and inherently broadens the range of spatial and temporal scales over which interactions occur.

Treating these myriad processes at device-relevant conditions requires significant trade-offs for both experiments and simulations. The highest quality experimental diagnostics provide only partial information. Modeling and simulation of these processes are always limited by computational power. Even with exascale computing (and beyond), direct numerical simulation (DNS) of the fully coupled equations of fluid motion, transport and chemical reaction can be applied only over a limited range of turbulence scales, at moderate Reynolds numbers, in highly canonical domains. Thus, treating the full range of time and length scales in practical configurations must always begin with some form of formal filtering of the governing conservation equations. The Reynolds-averaged Navier-Stokes (RANS) approximation, for example, employs filtering in time to derive the governing conservation equations for the mean state. For this approach all dynamic degrees of freedom smaller than the largest energy containing eddies in a flow are averaged and no information exists to describe interactions between the small scales. The large eddy simulation (LES) technique, on the other hand, has historically employed spatial filtering to split field variables into time-dependent resolved-scale and subgrid-scale (SGS) components. In the most general case, LES can also accommodate temporal filtering to account for SGS fluctuations in time.

The basic trade-off between RANS, LES, and DNS is one of accuracy versus computational expense. All three methods begin with the same set of governing conservation equations. RANS is currently the primary method used for industry relevant engineering calculations since it is the least costly. However, models associated with RANS closures must represent dynamic interactions over the full range of spatial and temporal scales in a flow to approximate the bulk average effect on the largest flow features. As a consequence, RANS models are the least universal in character, involve many tuning constants, and must be calibrated on a case by case basis. DNS, on the other hand, requires no turbulence models but is well known to be limited by the extreme computational requirements of resolving the smallest turbulence or flame scales in a flow. This limits the application of DNS to canonical flows at moderate Reynolds numbers aimed at fundamental understanding of small-scale turbulence-chemistry interactions. Such approximations have limited degrees of relevance to the actual conditions of interest in a given device and thus provide only an indirect means to validate various models.

LES provides a compromise between the extreme limits of RANS and DNS but requires SGS models. Just as one chooses the resolution for a photographic image, one can conceptually choose the resolution for pertinent broadband structures of a flow if validated models are available that accurately represent the selected band of SGS processes. As the resolution is increased, the cost of a calculation increases; but the range of scales over which the SGS models must work becomes proportionately less, and they tend to be more universal in character. The mathematical formalism of LES also facilitates use of powerful identities associated with filtering that eliminate tuning constants leaving the specification of boundary conditions, grid resolution, and integration time-step as the only adjustable parameters. Given these attributes, LES can span a range of scales from the DNS limit to RANS and can be used as a tool for both scientific discovery (using higher-fidelity, albeit more expensive “science-based” models) and engineering design (using less expensive, albeit less universal “engineering-based” models). The approach here involves the former.

This paper provides an overview of progress to date in the application of high-fidelity LES for propulsion and power applications. Our approach is focused on the needs listed in Table 1 and involves four basic steps: (1) establish complementary links between basic and applied research programs; (2) establish close coordination with related target experiments aimed at model validation; (3) continue to build our theoretical-numerical capabilities through development of advanced SGS models; and (4) maximize the benefits of high performance computing through close collaborations with key DOE computational facilities. All of the cases considered involve the common objective of establishing a one-to-one correspondence with key target experiments while adhering to the strictest accuracy requirements for LES. These requirements include use of clean numerics (e.g., nondissipative spatial stencils with no artificial dissipation terms), high-quality grids, and science-based SGS models that take full advantage of the LES formalism and are designed for high-resolution applications.

Table 1: Basic needs for development of advanced simulation technologies for propulsion and power systems.

---

**1. Hierarchical model development, validation, and reduction:**

Benchmark experiments using advanced laser diagnostics for model validation data.  
High-fidelity LES that identically matches experiments for detailed model development.  
Tandem engineering-LES and/or RANS to establish predictive and affordable design tools for industry.

**2. Submodel development:**

Fuel injection and atomization.  
Multiphase flow and spray dynamics.  
High-pressure (supercritical) phenomena.  
Turbulent mixed-mode combustion, complex geometry.  
Detailed and reduced chemical kinetics.

**3. Tool infrastructure development:**

Advanced grid generation and grid quality assessment.  
Advanced model reduction techniques and uncertainty quantification.  
Postprocessing, visualization, data management for both science and engineering.

---

## 2. Programmatic Links between Basic and Applied Research

Several aspects distinguish our research from typical approaches. All the LES calculations performed reach beyond the capabilities and resources of most universities and industry and are consistent with a national laboratory's role of using high-performance computing to enable fundamental exploration of complex phenomena. We apply a single, unified theoretical-numerical framework (called "RAPTOR") to all cases being considered. This framework is completely general and has been optimized to handle high-Reynolds-number, high-pressure, real-gas and/or liquid conditions over a wide Mach operating range (from incompressible, through transonic, to supersonic conditions) and a wide envelope of thermophysical conditions. The numerical algorithm is massively parallel and has been optimized to meet the strict algorithmic requirements imposed by the LES formalism. It is designed to handle state-of-the-art grids and complex geometries and employs a general R-refinement adaptive mesh capability. This allows us to account for the inherent effects of geometry on turbulence over the full range of relevant scales while significantly reducing the total number of grid cells required (i.e., the cost) for a given calculation. Details related to the theoretical formulation are given by Oefelein [1] and described further below.

Over the past several years we have been highly successful in linking our LES activities with a synergistic combination of basic-science and applied-engineering research programs. An example of two key projects enabled is given in Fig. 1. The first is sponsored by the DOE Office of Science (SC), Basic Energy Sciences (BES) program, and focuses on LES of turbulence-chemistry interactions in reacting multiphase flows. The second is sponsored by the Energy Efficiency and Renewable Energy (EERE), Office of Vehicle Technologies (OVT) program, and focuses on the application of LES to advanced engine combustion research. Objectives and milestones for both projects are aimed at establishing high-fidelity computational benchmarks that identically match the geometry and operating conditions of key target experiments. To the left in Fig. 1 is a subset of turbulent flames being studied as part of the BES program. To the right is a subset of experiments associated with the OVT program. The projects are complementary in that BES-funded research provides the basic science foundation for advanced model development, while OVT-funded research provides the applied component for advanced engine development. This combination of projects directly addresses targeted research areas identified as part of a BES-sponsored workshop entitled *Basic Research Needs for Clean and Efficient Combustion of 21st Century Transportation Fuels* [2].

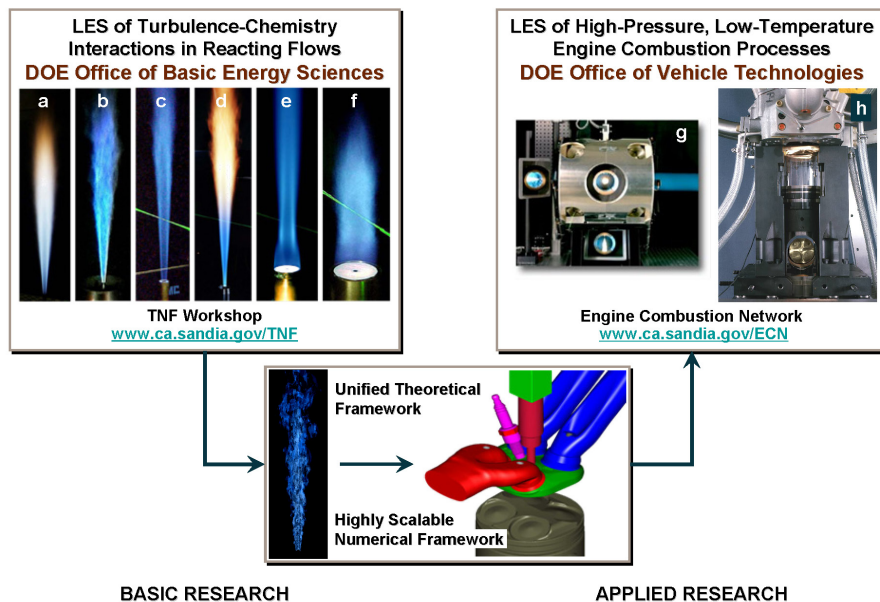


Figure 1: Advanced capabilities in LES provide a programmatic link between basic and applied sciences. A subset of turbulent flames associated with the BES Experimental Reacting Flow Research program are shown on the left (a,b: Simple jet flames, c,d: Piloted jet flames, e: Bluff-body; f: Bluff-body with swirl). A subset of experiments associated with the OVT Advanced Engine Combustion program is shown on the right (g: High-pressure combustion vessel, h: Typical single-cylinder optically accessible internal combustion engine).

### 3. Advances in High-Performance Computing

DOE has made significant investments in high-performance computing (HPC) facilities over the past several years while at the same time recognizing that a hierarchy of both local and national resources is necessary to support computationally intensive research. Progress depends on ready access to all parts of that hierarchy and on the complementary integration of its components, both internally and among centers. This notion was effectively expressed in a seminal report in 1993 to the National Science Foundation titled *Exploiting the Lead in High Performance Computing* by L. Branscomb (NSB 93-205, August 1993) and was reiterated by the DOE Basic Energy Sciences Advisory Committee in an Office of Science report titled *Opportunities for Discovery: Theory and Computation in Basic Energy Sciences* in January 2005 [3]. Since this time we have systematically pursued the development of an optimal hierarchy of resources to maximize the benefits of HPC for turbulent combustion research.

Our efforts to combine state-of-the-art LES, experiments, and HPC over the past several years has catalyzed significant growth and collaborative opportunities. Much of this growth has been facilitated by establishing our local Computational Combustion and Chemistry Laboratory. The dedicated local-capacity clusters provide a significant production-level computing capability for routine calculations and serve as staging platforms for more efficient use of large-scale computing facilities such as the Lawrence Berkeley National Laboratory (LBNL), National Energy Research Scientific Computing Center (NERSC) ([www.nersc.gov](http://www.nersc.gov)), and the Oak Ridge National Laboratory (ORNL), National Center for Computational Science (NCCS) ([www.nccs.gov](http://www.nccs.gov)). Using our local mid-scale systems in concert with grants such as the Innovative and Novel Computational Impact on Theory and Experiment (INCITE) ([www.sc.doe.gov/ascr/incite](http://www.sc.doe.gov/ascr/incite)) has enabled access to the full hierarchy of computing resources needed for state-of-the-art combustion simulations.

#### 4. Development of a Generalized Theoretical-Numerical Framework

Using the hierarchy of HPC resources described above to its full potential requires the development of specialized massively parallel flow solvers that can be easily ported to a variety of platforms and scale efficiently on  $\mathcal{O}(10^5)$  processing cores and beyond. From this perspective, the approach described above has been enabled through a unique theoretical-numerical framework, called RAPTOR, developed over the past 18 years. Unlike conventional LES solvers (which are typically based on the low-Mach-number fractional-step methodology), RAPTOR is a massively parallel DNS solver that has been designed specifically for application of LES to turbulent, chemically reacting, multiphase flows in complex geometries. It solves the fully coupled conservation equations of mass, momentum, total energy, and species for a chemically reacting system. It also accounts for detailed thermodynamics and transport processes at the molecular level. The code is sophisticated in its ability to handle complex geometries and a generalized SGS model framework. It treats spray combustion processes and other particulate flows using a Lagrangian-Eulerian formulation. The theoretical framework handles both multicomponent and mixture-averaged systems and employs a general treatment of the equation of state, thermodynamics, and transport properties. The code is designed to handle high-pressure, high-Reynolds number flows over a wide Mach operating envelope (both compressible and incompressible). It accommodates real gases or liquids and is not constrained to ideal gas applications.

##### 4.1. Governing Conservation Equations

For LES applications the instantaneous conservation equations are filtered, yielding the following:

- Mass:

$$\frac{\partial}{\partial t}(\theta\bar{\rho}) + \nabla \cdot (\theta\bar{\rho}\tilde{\mathbf{u}}) = \bar{\rho}_s. \quad (1)$$

- Momentum:

$$\frac{\partial}{\partial t}(\theta\bar{\rho}\tilde{\mathbf{u}}) + \nabla \cdot \left[ \theta \left( \bar{\rho}\tilde{\mathbf{u}} \otimes \tilde{\mathbf{u}} + \frac{\mathcal{P}}{M^2}\mathbf{I} \right) \right] = \nabla \cdot (\theta\vec{\mathcal{T}}) + \bar{\mathbf{F}}_s. \quad (2)$$

- Total Energy:

$$\frac{\partial}{\partial t}(\theta\bar{\rho}\tilde{e}_t) + \nabla \cdot [\theta(\bar{\rho}\tilde{e}_t + \mathcal{P})\tilde{\mathbf{u}}] = \nabla \cdot \left[ \theta \left( \bar{Q}_e + M^2(\vec{\mathcal{T}} \cdot \tilde{\mathbf{u}}) \right) \right] + \theta\bar{Q}_e + \bar{Q}_s. \quad (3)$$

- Species:

$$\frac{\partial}{\partial t}(\theta\bar{\rho}\tilde{Y}_i) + \nabla \cdot (\theta\bar{\rho}\tilde{Y}_i\tilde{\mathbf{u}}) = \nabla \cdot (\theta\vec{\mathcal{S}}_i) + \theta\bar{\omega}_i + \bar{\omega}_{s_i}. \quad (4)$$

The terms  $\theta$ ,  $\bar{\rho}_s$ ,  $\bar{\mathbf{F}}_s$ ,  $\bar{Q}_s$ , and  $\bar{\omega}_{s_i}$  represent the filtered void fraction and spray source terms that account for exchange of mass, momentum, total energy, and species, respectively. The terms  $\mathcal{P}$ ,  $\vec{\mathcal{T}}$ ,  $\bar{Q}_e$ , and  $\vec{\mathcal{S}}_i$  represent respective composite (i.e., molecular plus SGS) stresses and fluxes. The terms  $\bar{Q}_e$  and  $\bar{\omega}_i$  represent the filtered energy and chemical source terms, respectively.

##### 4.2. Baseline Subgrid-Scale Closure

The baseline SGS closure is obtained using the ‘‘mixed’’ dynamic Smagorinsky model by combining the models proposed by Erlebacher, Hussaini, Speziale, and Zang [4] and Speziale [5] with the dynamic modeling procedure [6, 7, 8, 9, 10]. The composite stresses and fluxes in Eqs. (1)–(4) are given as

$$\vec{\mathcal{T}} = (\mu_t + \mu) \frac{1}{Re} \left[ -\frac{2}{3}(\nabla \cdot \tilde{\mathbf{u}})\mathbf{I} + (\nabla\tilde{\mathbf{u}} + \nabla\tilde{\mathbf{u}}^T) \right] - \bar{\rho} \left( \tilde{\mathbf{u}} \otimes \tilde{\mathbf{u}} - \tilde{\omega} \otimes \tilde{\mathbf{u}} \right), \quad (5)$$

$$\vec{Q}_e = \left( \frac{\mu_t}{Pr_t} + \frac{\mu}{Pr} \right) \frac{1}{Re} \nabla \tilde{h} + \sum_{i=1}^N \tilde{h}_i \vec{S}_i - \bar{\rho} \left( \tilde{h} \tilde{\mathbf{u}} - \tilde{h} \tilde{\mathbf{u}} \right), \text{ and} \quad (6)$$

$$\vec{S}_i = \left( \frac{\mu_t}{Sc_{t_i}} + \frac{\mu}{Sc_i} \right) \frac{1}{Re} \nabla \tilde{Y}_i - \bar{\rho} \left( \tilde{Y}_i \tilde{\mathbf{u}} - \tilde{Y}_i \tilde{\mathbf{u}} \right). \quad (7)$$

Here, the term  $\mu_t$  represents the SGS eddy viscosity given by the relation

$$\mu_t = \bar{\rho} C_R \Delta^2 \Pi_{\tilde{\mathbf{S}}}^{\frac{1}{2}}, \quad (8)$$

where

$$\Pi_{\tilde{\mathbf{S}}} = \tilde{\mathbf{S}} : \tilde{\mathbf{S}}, \text{ and } \tilde{\mathbf{S}} = \frac{1}{2} \left( \nabla \tilde{\mathbf{u}} + \nabla \tilde{\mathbf{u}}^T \right). \quad (9)$$

The terms  $C_R$ ,  $Pr_t$ , and  $Sc_{t_i}$  represent the Smagorinsky, SGS-Prandtl and SGS-Schmidt numbers and are evaluated dynamically as functions of space and time. Thus, no tuned constants are employed anywhere in the closure. The overall model includes the Leonard and cross-term stresses and provides a Favre averaged generalization of the Smagorinsky eddy viscosity model [11] coupled with gradient diffusion models that simulate SGS mass and energy transport processes.

#### 4.3. Thermodynamic and Transport Properties

The property evaluation scheme is designed to account for thermodynamic nonidealities and transport anomalies over a wide range of pressures and temperatures. The scheme is comprehensive and intricate; thus only a skeletal description can be given here. The extended corresponding states model [12, 13] is employed with a cubic equation of state. In past studies [14, 15] modified versions of both the Benedict-Webb-Rubin (BWR) equation of state and cubic equations of state have been used to evaluate the pressure-volume-temperature (PVT) behavior of dense multicomponent multiphase mixtures. Use of modified BWR equations of state in conjunction with the extended corresponding states principle has been shown to provide consistently accurate results over the widest range of pressures, temperatures, and mixture states, especially at near-critical conditions. A major disadvantage of BWR equations, however, is that they are computationally expensive.

Cubic equations of state can be less accurate, especially for mixtures at near-critical or saturated conditions, but are computationally efficient. Experience has shown that both the Soave-Redlich-Kwong (SRK) and Peng-Robinson (PR) equations, when used in conjunction with the corresponding states principle, can give accurate results over a wide range of pressures, temperatures, and mixture states of typical interest in a variety of devices. SRK coefficients are fit to vapor pressure data and are thus more suitable for conditions when the reduced temperature is less than one. PR coefficients, on the other hand, are more suitable for conditions when the reduced temperature is greater than one. The cubic equations of state and recommended constants are given by Reid *et al* [16, Chapter 3].

Having established an analytical representation for real mixture PVT behavior, the thermodynamic properties are obtained in two steps. First, respective component properties are combined at a fixed temperature by using the extended corresponding states methodology outlined above to obtain the mixture state at a given reference pressure. A pressure correction is then applied using departure functions of the form given by Reid *et al* [16, Chapter 5]. These functions are exact relations derived by using the Maxwell relations (see VanWylen and Sonntag [17, Chapter 10], for example) and make full use of the real mixture PVT path dependencies dictated by the equation of state. Standard state properties are obtained by using the databases developed by Gordon and McBride [18] and Kee *et al*. [19]. Chemical potentials and fugacity coefficients are obtained in a manner similar to that outlined above.

Molecular transport properties are evaluated in a manner analogous to the thermodynamic properties. Viscosity and thermal conductivity are obtained by using the extended corresponding states methodologies developed by Ely and Hanley [20, 21]. The mass diffusion coefficients and thermal diffusion coefficients are obtained using the methodologies outlined by Bird *et al.* [22] and Hirschfelder *et al.* [23] in conjunction with the corresponding states methodology proposed by Takahashi [24].

#### 4.4. Numerical Framework

The temporal integration scheme employs an all-Mach-number formulation using dual time-stepping with generalized preconditioning. The approach is fourth-order accurate in time and provides a fully implicit solution using a fully explicit (highly scalable) multistage scheme. Preconditioning is applied on an inner pseudo-time loop and coupled to local time-stepping techniques to minimize convective, diffusive, geometric, and source term anomalies (i.e., stiffness) in an optimal manner. This maximizes convergence rates as the system is advanced in time. The formulation is A-stable, which allows one to set the physical time-step based solely on accuracy considerations. This attribute typically provides a 2 to 3 orders of magnitude increase in the allowable integration time-step compared to conventional compressible flow solvers, especially in the low Mach number regime.

The spatial scheme is designed using nondissipative, discretely conservative, staggered, finite-volume differencing. The discretization is formulated in generalized curvilinear (i.e., body-fitted) coordinates and employs a general R-refinement adaptive mesh capability. This allows us to account for the inherent effects of geometry on turbulence over the full range of relevant scales while significantly reducing the total number of grid cells required in the computational domain. The differencing methodology has been specifically designed for LES. In particular, the second-order accurate staggered grid formulation (where we store scalar values at cell centers and velocity components at respective cell faces) fulfills two key accuracy requirements. First, it is spatially nondissipative, which eliminates numerical contamination of the SGS models due to artificial dissipation. Second, the stencils provide discrete conservation of mass, momentum, total energy, and species, which eliminates the artificial build up of velocity and scalar energy at the high wavenumbers. The algorithm includes appropriate switches to handle shocks, detonations, flame fronts, and contact discontinuities.

The RAPTOR code framework is massively parallel and has been optimized to provide excellent parallel scalability attributes using a distributed multiblock domain decomposition with a generalized connectivity scheme. Distributed-memory message passing is performed with MPI and the single-program-multiple-data (SPMD) model. It accommodates complex geometric features and time-varying meshes with generalized hexahedral cells while maintaining the high-accuracy attributes of structured spatial stencils. The numerical framework has been ported to all major platforms and provides highly efficient coarse- and fine-grained (i.e., weak and strong) scalability attributes. The code has been optimized for both vector and commodity architectures. We continue to perform a combination of validation and performance studies to maintain the accuracy and computational efficiency of the code. A suite of sample results associated with our validation efforts is shown in Fig. 2. Representative case studies are given by Oefelein *et al.* [14, 25, 15, 26, 27, 28, 29, 30, 31, 32, 33].

In 2009, RAPTOR was selected as one of the application codes to be evaluated under the DOE Office of Advanced Scientific Computing Research (ASCR) annual *Joule Metric on Computational Effectiveness*. A key element of this program was to evaluate the existing baseline performance of the code and demonstrate that it scaled linearly on DOE capability-class computers. In order to achieve this goal, a series of weak-scaling studies were performed to demonstrate the combined computational effectiveness of the ORNL NCCS Cray-XT platform (Jaguar) and RAPTOR. The first step toward measuring the performance was defining a realistic model problem that was representative of actual production simulations. For this study, we chose the turbulent nonpremixed  $\text{CH}_4/\text{H}_2/\text{N}_2$  jet flame known as the “DLR-A” configuration. A photograph of this flame is shown in Fig. 1b and in Fig. 2 (i.e., see “Nonpremixed Flames”); also see [34]. Using this configuration, we successfully demonstrated that the code scaled linearly beyond 150,000 processor cores for extremely fine-grained problems. Details

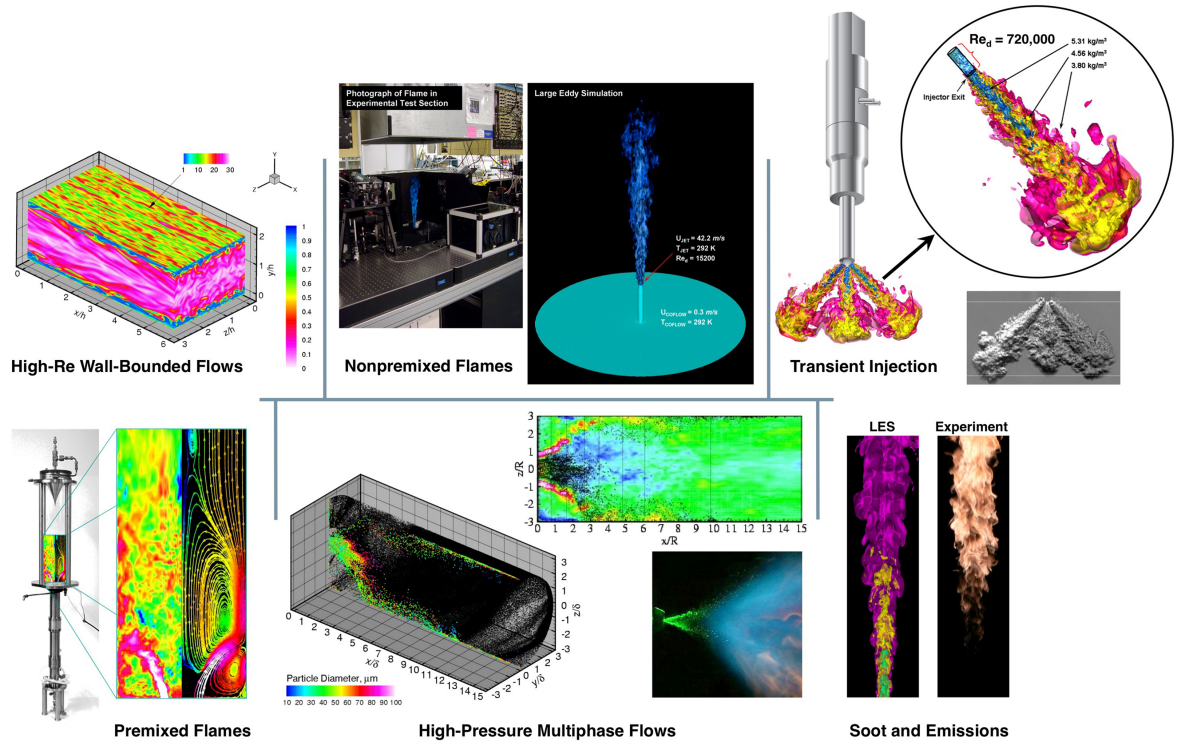


Figure 2: RAPTOR has been validated for a wide range of turbulent reacting multiphase flows.

related to this activity can be found in the report by Kothe *et al.* [35] and paper by Oefelein and Sankaran [36].

For LES, it is also important to demonstrate the code has efficient strong-scaling attributes. The strong-scaling attributes of RAPTOR from a recent test on Jaguar are shown in Fig. 3. For this test we started with a single block (serial) grid of 1.28-million cells, then successively increased the number of cores with the total grid size fixed to determine the net speedup. Note that the case shown here represents the most severe condition, where at 20,000 cores we have only  $4^3$  cells per block but still maintain over 80 percent parallel efficiency. This is an extremely fine-grained test. Under more typical conditions, RAPTOR exhibits parallel efficiencies well above 90 percent.

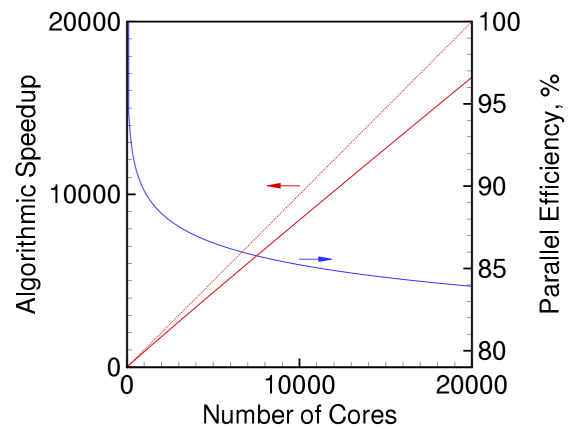


Figure 3: Strong (fine-grained) scaling attributes exhibited by RAPTOR on Jaguar.

## 5. Representative Case Studies

### 5.1. Model Validation using TNF Workshop Flames

Considerable progress has been made in the application of LES to inert flows. Early works relied heavily on the Smagorinsky model [11], and significant breakthroughs resulted from development of the dynamic modeling procedure [6, 8, 9, 10]. This procedure applies an exact mathematical identity (the “Germano identity”), which effectively replaces model constants with dynamic coefficients.

Table 2: Grid designed using the measured dissipation cutoff wavelengths (A) and two additional grids obtained by successively coarsening A by a factor of 2 in each coordinate direction (B and C, respectively).

Grid	Downstream of Jet Exit Plane			Total	Total Cells	$\Delta t$
	$N_{axial}$	$N_{radial}$	$N_{azimuthal}$			
A	2592	144	192	71,663,616	82,280,448	0.25 $\mu s$
B	1296	72	96	8,957,952	10,285,056	0.50 $\mu s$
C	648	36	48	1,119,744	1,285,632	1.00 $\mu s$

These coefficients are evaluated as functions of space and time in a manner that conceptually provides appropriate local levels of SGS mixing and dissipation. Dynamic modeling, coupled with scale similarity ideas, has been useful in modeling nonreacting flows. Our modeling approach makes use of this foundational body of work. The current SGS closure is obtained using the dynamic Smagorinsky model by combining the methods proposed by Erlebacher *et al.* [4] and Speziale [5] with the dynamic modeling procedure. No tuned constants are used anywhere in the closure and the only controlling parameters are grid spacing and boundary conditions.

Extension of the ideas above to reacting flows is still an active area of research. Progress and unresolved issues have been systematically documented over the past several years [37, 38, 39, 40, 41]. Most combustion models have been carried over from the engineering sector (i.e., RANS). Closures for nonpremixed combustion include laminar flamelet models [42, 43, 44, 45, 46], the conditional moment closure (CMC) model [47, 48, 49, 50, 51], probability density function (PDF) transport models [52, 53, 54, 55, 56, 57, 58, 59], the linear eddy model (LEM) [60, 61, 62, 63, 64, 65, 66, 67, 68], and its successor the one dimensional turbulence (ODT) model [69]. Closure schemes for premixed flames include application of the G-equation [70, 71, 72], surface density equations [73, 74], the thickened flame model [75], and LEM [76, 77]. All these models are engineering-based in that they employ assumptions that do not relax in the limit as the grid resolution and time-step approach the smallest relevant scales (i.e., the limit of a DNS). Here we describe a new modeling approach that uses a stochastic reconstruction methodology to treat detailed chemistry directly within the LES formalism. This model is science-based in that it facilitates direct treatment of turbulence-chemistry interactions in a manner consistent with the application of DNS.

Recently, a class of reconstruction models has been proposed [78, 79] that combines the purely mathematical approximate deconvolution procedure with physical information from an assumed scalar spectrum. With this method, a surrogate to the exact scalar field can be estimated such that filtered moments match to a specified order. In principle, the surrogate field can be used to calculate the SGS contribution of any related nonlinear function. In practice, however, the extent of the nonlinearity limits the accuracy, and it has been shown that the method cannot be used reliably to close the filtered chemical source terms directly. It can be used, on the other hand, to obtain highly accurate representations of polynomial nonlinearities such as the SGS scalar variances. These are precisely the inputs required to generate SGS fluctuations stochastically. Given these findings, we have proposed an extension to this approach by coupling it to a stochastic reconstruction technique. The matrix of SGS variances are used as input to a Cholesky decomposition to obtain a correlated approximation of SGS velocity and scalar fluctuations with the correct time history and spatial distribution. The modeled instantaneous fields (i.e.,  $\phi_i = \tilde{\phi}_i + \phi_i''$ , where  $\tilde{\phi}_i$  represents the resolved-scale contribution of an arbitrary scalar and  $\phi_i''$  the correlated SGS fluctuation) are used to evaluate the filtered chemical source terms directly. The filtered source terms are closed by selecting an appropriate chemical kinetic mechanism in the same manner as is done for DNS. Model coefficients are evaluated locally in a manner consistent with the dynamic modeling procedure. The only adjustable parameters are the grid resolution, integration time-step, and boundary conditions. In the limit as the grid resolution and time-step approach the smallest relevant scales, SGS contributions approach zero, and the solution converges to a DNS.

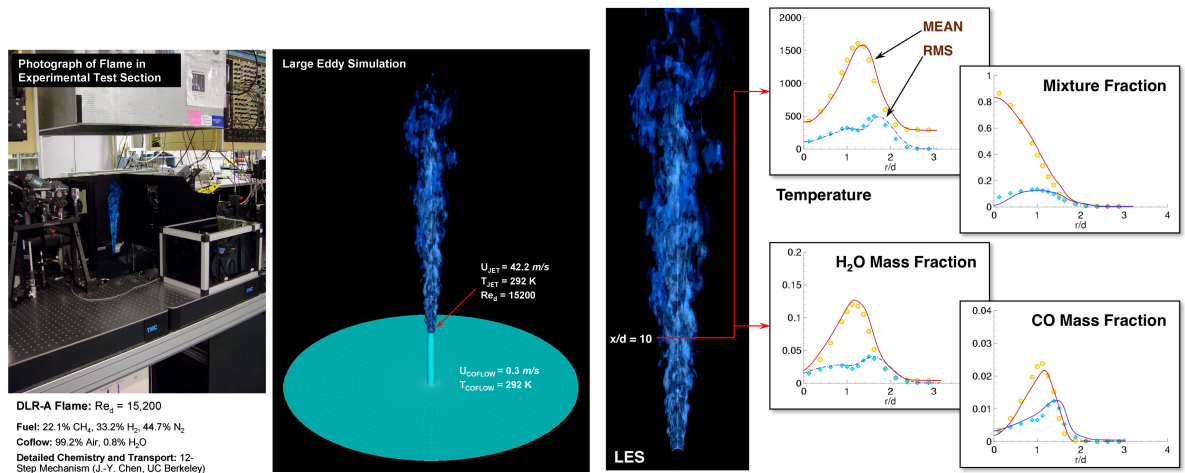


Figure 4: At left is a photograph of the DLR-A flame in the experimental test section. At center is a corresponding solution from LES. At right are representative comparisons between experimentally measured (symbols) and modeled (lines) results showing good agreement.

In order to establish the baseline accuracy of the model and study the related issues of scalar mixing, we performed an LES of the DLR-A flame by using the 12-step 16-species reduced chemical mechanism for methane-air developed by J.-Y. Chen (U.C. Berkeley). The computational domain is shown in Fig. 2 (see center image labeled “Nonpremixed Flames”). To eliminate ambiguities associated with boundary conditions, the computational domain includes the entire experimental test section and burner geometry. The inner jet diameter is 8.0 mm. The outer nozzle surface is tapered to a sharp edge at the burner exit. The overall domain dimensions are 110 by 40 jet diameters (88 cm  $\times$  32 cm). The jet nozzle itself is 10 diameters long. Cells upstream of the jet exit are clustered inside the jet nozzle to accurately treat the turbulent time-dependent boundary layer, and outside the burner to accurately treat the coflow of air that surrounds the burner. A novel feature of our approach was to design the LES grids using the measured dissipation spectrum cutoff-length scales provided by Frank *et al.* [80, 81]. For the baseline case considered here, we used Grid B listed in Table 2.

The bulk jet and coflow velocities for the DLR-A case are 42.2 and 0.3 m/s, respectively. The burner section is long enough to assume that a fully developed turbulent profile exists inside the jet nozzle. With the added assumption that all wall surfaces are hydraulically smooth, we use the LES solver itself to drive a fully-developed turbulent boundary layer inside the duct. Time-evolving velocity profiles are generated by recycling the fields from radial planes at an axial distance of two dimensionless units upstream of the jet exit. The stripped fields are then imposed at the burner inlet 10 units upstream along with a nonreflecting pressure condition. Far-field, force-free conditions are imposed elsewhere. Figure 4 shows a set of representative results. At the left is a photograph of the DLR-A flame in the experimental test section. At the center is a corresponding instantaneous solution from LES. At the right are representative comparisons between measured Raman/Rayleigh/CO-LIF line images (symbols) and modeled mean and RMS profiles (lines). The agreement is good in all cases.

In general, the integral-scale Reynolds number for the DLR-A flame (and other TNF flames) are of  $\mathcal{O}(10^4)$ , whereas those associated with most propulsion and power devices are of  $\mathcal{O}(10^5)$  or greater. Thus, the agreement in Fig. 4 with respect to the mean and RMS profiles is a necessary but not sufficient condition for determining the merits of the model. There is a clear need to quantify the effects of increasing Reynolds number on turbulent flame dynamics and understand how LES represents the related scalar-mixing processes as a function of grid resolution. From this perspective, the coupling of imaging diagnostics and LES provides a unique opportunity for understanding turbulence-flame

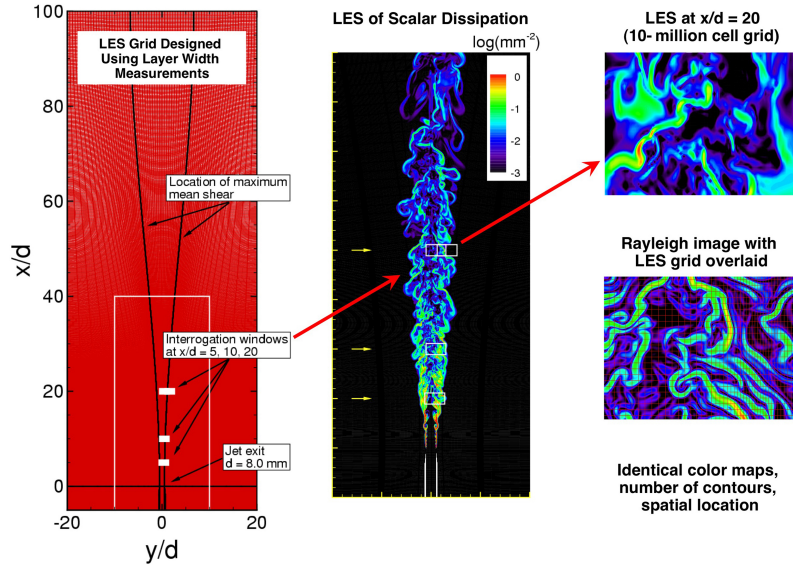


Figure 5: At left is a cross-section of Grid B (see Table 2) showing key topological features and the location of the imaging windows. At center is the instantaneous structure of the dissipation field from LES. At right is a close-up of the dissipation structure from LES at  $x/d = 20$  compared with an experimental image.

interactions and the related structural dynamics of mixing. High-resolution imaging of turbulent jet flames has provided insights into the dynamic structure of the thermal dissipation field [80, 81]. These insights have motivated studies of scalar mixing in nonreacting jets over the same range of Reynolds numbers as the DLR-A flame, using the same geometry.

The images of the thermal and scalar dissipation fields acquired by Frank *et al.* [80, 81] have revealed the convoluted inhomogeneous structure of the small-scale scalar mixing processes. The orientation and morphology of the structures are anisotropic and vary significantly from the low-temperature regions near the jet centerline to the high-temperature reaction zone. Using these data, we have performed a systematic analysis of the instantaneous structures and, as a first step, optimized a set of LES grids using the measured dissipation spectrum cutoff length scales. Table 2 summarizes the key attributes. We constructed the baseline, Grid A, by applying local spacing in all three coordinate directions that nominally matches the measured dissipation cutoff wavelengths. Grids B and C were then obtained by successively coarsening Grid A by a factor of 2 in each coordinate direction. This produced grids with approximately 82 million, 10 million, and 1.3 million cells, respectively, while maintaining the optimized stretching topology. Using these grids, we performed a series of LES calculations at conditions that identically match the experiments. Calculations were carried out initially using Grid C with a time-step of  $1 \mu s$ . Calculations performed using Grids B and A were integrated using time-steps of  $0.5$  and  $0.25 \mu s$ , respectively, in a manner consistent with the spatial refinement.

A cross-section of Grid B with key topological features and the location of the imaging windows is shown in Fig. 5 along with the corresponding instantaneous structure of the dissipation field from LES (center). To the right is a close-up of the dissipation structures from LES at  $x/d = 20$  compared with a corresponding experimental image with Grid B overlaid. Overlaying the local grid spacing on the actual measured images provides a revealing picture. In both nonreacting jets and flames, the dissipation field consists of elongated and convoluted filaments. These structures span multiple LES cells in the longitudinal direction and are of the same order of magnitude as the grid spacing in the transverse direction. The morphology and size relative to even the coarsest grid suggest that the LES must account for the overlap of dissipation structures in both the subgrid and resolved scales. The limited quantity of dissipation structures in each LES grid cell also suggests that widely used assumptions regarding the

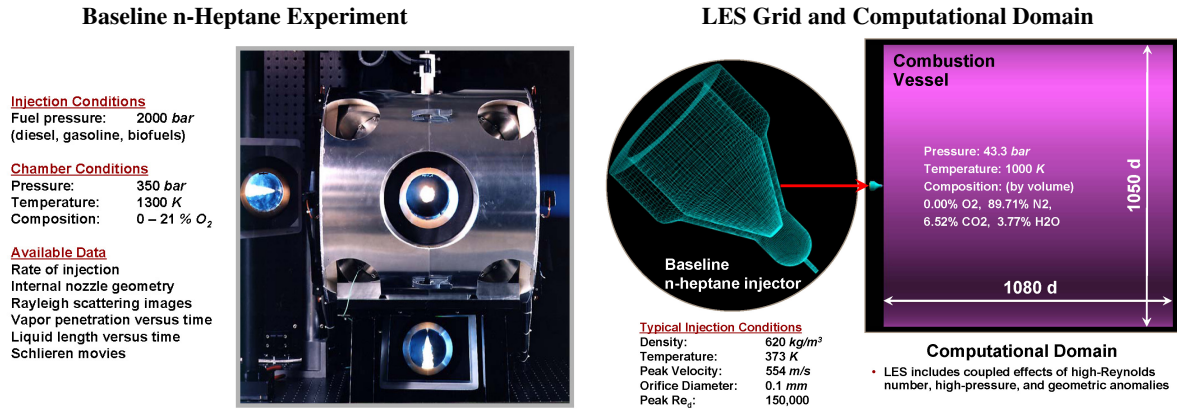


Figure 6: Photograph of the Sandia high-pressure combustion vessel (left) and computational domain (right) used for LES of the baseline n-heptane injector configuration. The injector is mounted at the head end of the vessel, as indicated by the red arrow. The grid and operating conditions identically match the experiment.

sampling of statistically significant quantities of turbulence structures within each grid cell, as well as the assumption of isotropy in the subgrid for treatment of scalar mixing, must be carefully examined. Findings to date have been reported by Frank, Kaiser, and Oefelein [32].

### 5.2. Analysis of Direct Injection Processes for Diesel Engine Applications

The importance of understanding and predicting fuel injection, atomization and dense spray dynamics in advanced engine systems is widely recognized. The difficulties in measuring spray phenomena, especially in the dense regime, are also well recognized. One aspect that is not as well understood is the effect of pressure on the fundamental physics of injection. Depending on the pressure, injected fuel jets exhibit two distinctly different sets of evolutionary processes. At subcritical cylinder pressures, the classical situation exists where a well-defined interface separates the injected liquid from ambient gases due to the presence of surface tension. Dynamic shear forces and surface tension promote primary atomization and secondary breakup processes that evolve from a very dense state, where the liquid exists as sheets filaments or lattices intermixed with sparse pockets of gas; to a very dilute state, where drop-drop interactions are negligible and the theory associated with isolated drops can be used. As chamber pressures exceed the critical pressure of the fuel, however, the situation becomes quite different. Under these conditions, a distinct gas-liquid interface does not exist. Instead, injected liquid jets undergo a transcritical change of state as interfacial fluid temperatures rise above the critical temperature of the local mixture. Effects of surface tension become diminished, and the lack of these intermolecular forces promotes diffusion-dominated mixing processes prior to atomization. The injected jets evolve in the presence of exceedingly large (but continuous) thermophysical gradients in a manner markedly different from the classical picture typically assumed.

Using RAPTOR, we have begun investigations of a new multiphase combustion model aimed at treating the high-pressure phenomena described above. We have performed a select series of studies focused on the treatment of transcritical injection dynamics. The primary goal is to understand basic details related to the extreme variations in density and other thermophysical properties and how to best treat these conditions from the perspective of modeling, numerics, and code performance. To facilitate the analysis, we considered the operating conditions associated with the baseline n-heptane experiment being studied in the high-pressure combustion vessel at Sandia National Laboratories by Pickett *et al.* [82]. These experiments provide a relevant set of operating conditions for diesel engines. LES calculations were performed by identically matching the experimental operating conditions, injector geometry, and combustion chamber using advanced models and gridding techniques. The experimental

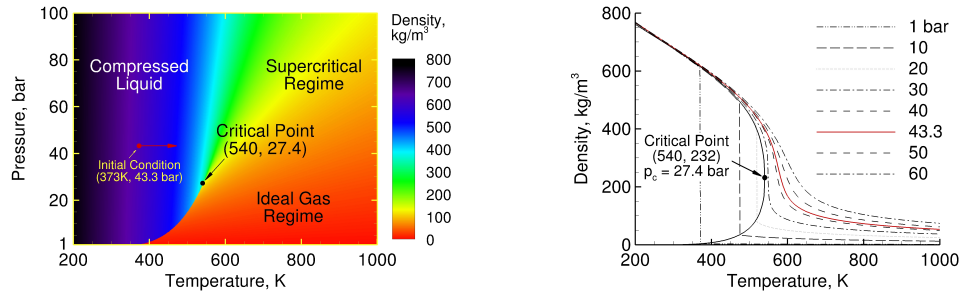


Figure 7: Thermodynamic characteristics of n-heptane showing key regimes and its initial state when injected into the combustion vessel. The jet enters as a compressed liquid and is heated at supercritical pressure.

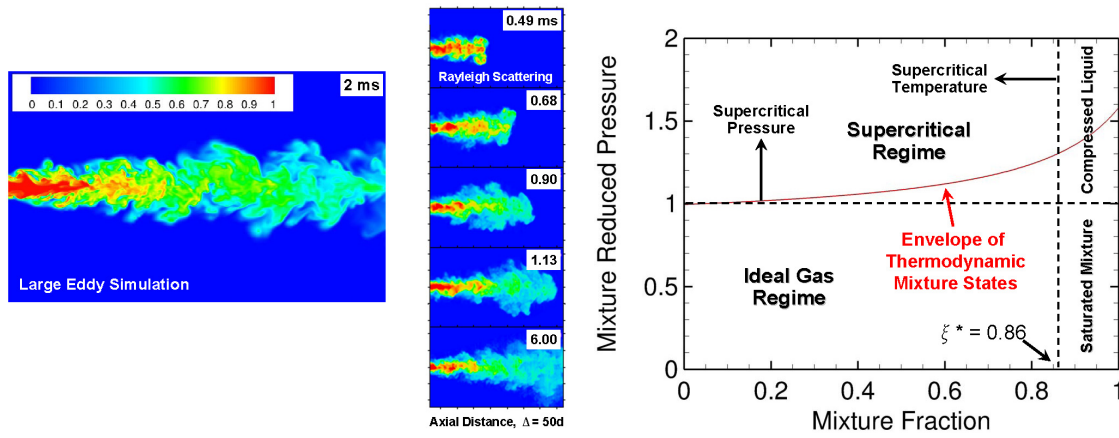


Figure 8: Comparison of the mixture fraction distribution from LES with measured Rayleigh images (left) and the envelope of mixture states predicted as a function of mixture fraction (right).

apparatus, corresponding computational domain, and key operating conditions used in the calculations are shown in Fig. 6. The experiment emulates conditions encountered in modern diesel engines and involves a liquid n-heptane jet injected into a hot quiescent mixture of gaseous products. For the case considered here, all the oxygen has been consumed to prevent the onset of combustion so we can focus on thermophysical processes associated with injection. The thermodynamic characteristics of n-heptane are shown in Fig. 7. Its critical point is  $540\text{ K}$ ,  $27.4\text{ bar}$ . Thus, liquid injection occurs at transcritical conditions (i.e., supercritical with respect to pressure, subcritical with respect to temperature).

Figure 8 provides a representative comparison of the mixture fraction distribution predicted using LES with the corresponding experimentally measured Rayleigh images. In general, predictions agree well with the available experimental data. The plot to the right shows the envelope of mixture states predicted as a function of mixture fraction. Current emphasis has been placed on development and validation of a property evaluation scheme designed to account for thermodynamic nonidealities and transport anomalies at the conditions described here [83, 84]. The primary focal point is on determining the degree to which thermodynamic nonidealities and transport anomalies play a role in the overall mixture preparation just prior to combustion. As one example of the findings to date, Fig. 9 shows a typical instantaneous LES field with isolines that mark the thermodynamic transition of the mixture from a compressed liquid to a supercritical state (black) and the separation between nonideal and ideal fluid behavior (white). These results demonstrate for the first time that the injected n-heptane enters the combustion chamber as a compressed liquid (not a spray) and is heated at supercritical pressure. Results indicate that applying the ideal gas assumption just prior to autoignition in these types of flows is not

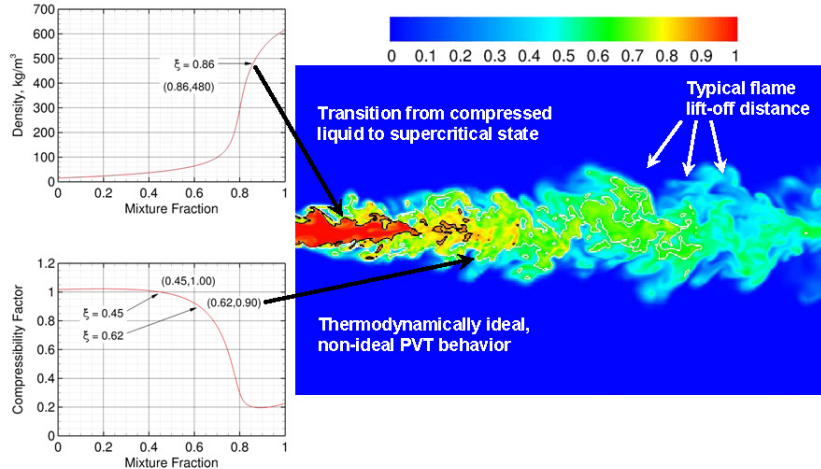


Figure 9: LES field with isolines that mark the transition of the mixture from a compressed liquid to supercritical state (black) and separation between regions of nonideal and ideal fluid behavior (white).

valid and the classical view of spray atomization, and secondary breakup processes as an appropriate model (as is widely assumed currently) is questionable. Instead, nonideal real-fluid behavior associated with the dense liquid jet must be taken into account.

## 6. Summary

An overview of progress to date in the application of high-fidelity LES for propulsion and power applications was presented. Our approach involves four basic steps: (1) establishing complementary links between basic and applied research programs, (2) establishing close coordination with related target experiments aimed at model validation, (3) continuing to build our theoretical-numerical capabilities through development of advanced SGS models, and (4) maximizing the benefits of high performance computing through close collaborations with key DOE computational facilities. All cases considered involve the common objective of establishing a one-to-one correspondence with key target experiments while adhering to the strictest accuracy requirements for LES. These requirements include use of clean numerics (e.g., nondissipative spatial stencils with no artificial dissipation terms, etc.), high-quality grids, and science-based SGS models designed for high-resolution applications that take full advantage of the LES formalism.

Studies to date address the need to resolve unsteady, highly nonlinear broadband transients, turbulence-chemistry interactions, and acoustic instabilities, all of which can have a profound effect on the operational characteristics of a given system. As part of our core effort, we will continue with the development of high-fidelity benchmark simulations in collaboration with companion experimental efforts. We will continue to develop and investigate the merits of a variety of SGS models for turbulent combustion. The focal point will include both analysis of existing models and new concepts such as the stochastic reconstruction model. In addition, there is a critical need for the development of quality assessment and uncertainty quantification techniques for LES. Initial activities have led to long term collaborations with Kempf (Imperial College London, UK) and Geurts (University of Twente, The Netherlands), with emphasis on application of the error-landscape methodology [33]. We are also collaborating with Najm [85], with emphasis on incorporating nonintrusive UQ methodologies into our LES framework.

## Acknowledgments

This work was supported by the United States Department of Energy (DOE), Office of Basic Energy Sciences, Division of Chemical Sciences, Geosciences, and Biosciences and the Office of Vehicle Technologies. Sandia National Laboratories is a multiprogram laboratory operated by Sandia Corporation, a Lockheed Martin Company, for the DOE under contract DE-AC04-94-AL85000. The work at Oak Ridge National Laboratory was supported by the DOE Office of Science under contract DE-AC05-00OR22725 and used resources of the National Center for Computational Sciences at ORNL. Computer time was granted under the Innovative and Novel Computational Impact on Theory and Experiment (INCITE) program.

## References

- [1] Oefelein J C 2006 *Progress in Aerospace Sciences* **42** 2–37
- [2] 2006 Basic research needs for clean and efficient combustion of 21st century transportation fuels [www.sc.doe.gov/bes/reports/files/CTF\\_rpt.pdf](http://www.sc.doe.gov/bes/reports/files/CTF_rpt.pdf) report of the Basic Energy Sciences Workshop on Clean and Efficient Combustion of 21st Century Transportation Fuels, U.S. Department of Energy
- [3] 2005 Opportunities for discovery: Theory and computation in basic energy sciences [www.sc.doe.gov/bes/reports/files/OD\\_rpt.pdf](http://www.sc.doe.gov/bes/reports/files/OD_rpt.pdf) subcommittee on Theory and Computation of the Basic Energy Sciences Advisory Committee, U.S. Department of Energy
- [4] Erlebacher G, Hussaini M Y, Speziale C G and Zang T A 1992 *Journal of Fluid Mechanics* **238** 155–185
- [5] Speziale C G 1985 *Journal of Fluid Mechanics* **156** 55–62
- [6] Germano M, Piomelli U, Moin P and Cabot W H 1991 *Physics of Fluids* **3** 1760–1765
- [7] Moin P, Squires K, Cabot W and Lee S 1991 *Physics of Fluids* **3** 2746–2757
- [8] Lilly D K 1992 *Physics of Fluids* **3** 633–635
- [9] Zang Y, Street R L and Koseff J R 1993 *Physics of Fluids* **5** 3186–3195
- [10] Vreman B, Geurts B and Kuerten H 1994 *Physics of Fluids* **6** 4057–4059
- [11] Smagorinsky J 1963 *Monthly Weather Review* **91** 99–164
- [12] Leland T W and Chappellear P S 1968 *Industrial and Engineering Chemistry Fundamentals* **60** 15–43
- [13] Rowlinson J S and Watson I D 1969 *Chemical Engineering Science* **24** 1565–1574
- [14] Oefelein J C 2005 *Proceedings of the Combustion Institute* **30** 2929–2937
- [15] Oefelein J C 2006 *Combustion Science and Technology* **178** 229–252
- [16] Reid R C, Prausnitz J M and Polling B E 1987 *The Properties of Liquids and Gases* 4th ed (New York, New York: McGraw-Hill)
- [17] VanWylen G J and Sonntag R E 1986 *Fundamentals of Classical Thermodynamics* 3rd ed (New York, New York: John Wiley and Sons, Incorporated)
- [18] Gordon S and McBride B J 1971 Computer program for calculation of complex chemical equilibrium compositions, rocket performance, incident and reflected shocks and Chapman-Jouguet detonations Tech. Rep. NASA SP-273 National Aeronautics and Space Administration
- [19] Kee R J, Rupley F M and Miller J A 1990 Chemkin thermodynamic data base Tech. Rep. SAND87-8215B Sandia National Laboratories supersedes SAND87-8215 dated April 1987
- [20] Ely J F and Hanley H J M 1981 *Industrial and Engineering Chemistry Fundamentals* **20** 323–332
- [21] Ely J F and Hanley H J M 1981 *Industrial and Engineering Chemistry Fundamentals* **22** 90–97
- [22] Bird R B, Stewart W E and Lightfoot E N 1960 *Transport Phenomena* (New York, New York: John Wiley and Sons, Incorporated)
- [23] Hirschfelder J O, Curtiss C F and Bird R B 1964 *Molecular Theory of Gases and Liquids* 2nd ed (New York, New York: John Wiley and Sons, Incorporated)
- [24] Takahashi S 1974 *Journal of Chemical Engineering of Japan* **7** 417–420
- [25] Oefelein J C, Schefer R W and Barlow R W 2006 *AIAA Journal* **44** 418–433
- [26] Oefelein J C, Sankaran V and Drozda T G 2007 *Proceedings of the Combustion Institute* **31** 2291–2299
- [27] Williams T C, Schefer R W, Oefelein J C and Shaddix C R 2007 *Review of Scientific Instruments* **78** 035114–1–9
- [28] Tucker P K, Menon S, Merkle C L, Oefelein J C and Yang V 2007 *43rd AIAA/ASME/SAE/ASEE Joint Propulsion Conference and Exhibit, Paper 2007-5572* Cincinnati, Ohio
- [29] Tucker P K, Menon S, Merkle C L, Oefelein J C and Yang V 2008 *44th AIAA/ASME/SAE/ASEE Joint Propulsion Conference and Exhibit, Paper 2008-5526* Hartford, Connecticut
- [30] Hu B, Musculus M P and Oefelein J C 2010 *SAE World Congress, Paper 2010-01-1133* Detroit, Michigan
- [31] Oefelein J C 2010 *CERFACS Colloquium on Multiphysics and Unsteady Simulations for Aeronautical Flows* Toulouse, France
- [32] Frank J H, Kaiser S A and Oefelein J C 2011 *Proceedings of the Combustion Institute* **33** 1373–1381

- [33] Kempf A M, Geurts B J and Oefelein J C 2011 *Combustion and Flame* Accepted
- [34] Barlow R S 1996-2011 International workshop on measurement and computation of turbulent (non)premixed flames [www.ca.sandia.gov/TNF](http://www.ca.sandia.gov/TNF) Combustion Research Facility, Sandia National Laboratories
- [35] Kothe D, Roche K, Kendall R, Adams M, Ahern S, Chang C S, Childs H, D'Azevedo E, Evans K, Evans T, Hack J, Klasky S, Ku S H, Oefelein J, Pugmire D, Rosinski J, Sankaran R and Worley P 2009 FY 2009 Annual report of joule software metric SC GG 3.1/2.5.2, improve computational science capabilities Tech. Rep. ORNL/TM-2009/322 Oak Ridge National Laboratory
- [36] Oefelein J C and Sankaran R 2009 *Proceedings of the 21st International Conference on Parallel Computational Fluid Dynamics* Moffett Field, California
- [37] Piomelli U 1999 *Progress in Aerospace Sciences* **35** 335–362
- [38] Bilger R W 2000 *Progress in Energy and Combustion Science* **26** 367–380
- [39] Veynante D and Vervisch L 2002 *Progress in Energy and Combustion Science* **28** 193–266
- [40] Janicka J and Sadiki A 2005 *Proceedings of the Combustion Institute* **30** 537–547
- [41] Pitsch H 2006 *Annual Review of Fluid Mechanics* **38** 453–482
- [42] Peters N 1984 *Progress in Energy and Combustion Science* **10** 319–339
- [43] Cook A W, Riley J J and Kosály G 1997 *Combustion and Flame* **109** 332–341
- [44] Cook A W and Riley J J 1998 *Combustion and Flame* **112** 593–606
- [45] DesJardin P E and Frankel S H 1998 *Physics of Fluids* **10** 2298–2314
- [46] Pitsch H and Steiner H 2000 *Physics of Fluids* **12** 2541–2554
- [47] Klimenko A Y 1990 *Fluid Dynamics* **25** 327–334
- [48] Bilger R W 1993 *Physics of Fluids* **5** 436–444
- [49] Klimenko A Y and Bilger R W 1999 *Progress in Energy and Combustion Science* **25** 595–687
- [50] Bushe W K and Steiner H 1999 *Physics of Fluids* **11** 1896–1906
- [51] Steiner H and Bushe W K 2000 *Physics of Fluids* **13** 754–769
- [52] Givi P 1989 *Progress in Energy and Combustion Science* **15** 1–107
- [53] Pope S B 1990 *Proceedings of the Combustion Institute* **23** 591–612
- [54] Colucci P J, Jaber F A, Givi P and Pope S B 1998 *Physics of Fluids* **10** 499–515
- [55] Jaber F A, Colucci P J, James S, Givi P and Pope S B 1999 *Journal of Fluid Mechanics* **401** 85–121
- [56] Gicquel L Y M, Givi P, Jaber F A and Pope S B 2002 *Physics of Fluids* **14** 1196–1213
- [57] Sheikhi M R H, Drozda T G, Givi P and Pope S B 2003 *Physics of Fluids* **15** 2321–2337
- [58] Sheikhi M R H, Drozda T G, Givi P, Jaber F A and Pope S B 2005 *Proceedings of the Combustion Institute* **30** 549–556
- [59] Givi P 2006 *AIAA Journal* **44** 16–23
- [60] Kerstein A R 1988 *Combustion Science and Technology* **60** 391–421
- [61] Kerstein A R 1989 *Combustion and Flame* **75** 397–413
- [62] Kerstein A R 1990 *Journal of Fluid Mechanics* **216** 411–435
- [63] Kerstein A R 1992 *Combustion Science and Technology* **81** 75–96
- [64] Kerstein A K 1991 *Physics of Fluids A* **3** 1110–1114
- [65] Kerstein A R 1991 *Journal of Fluid Mechanics* **231** 361–394
- [66] Kerstein A R 1992 *Journal of Fluid Mechanics* **240** 289–313
- [67] McMurtry P A, Menon S and Kerstein A R 1993 *Energy and Fuels* **7** 817–826
- [68] Kim W W, Menon S and Mongia H C 1999 *Combustion Science and Technology* **143** 25–62
- [69] Kerstein A R 1999 *Journal of Fluid Mechanics* **392** 277–334
- [70] Kim W W and Menon S 2000 *Combustion Science and Technology* **160** 119–150
- [71] Knikker R, Veynante D and Meneveau C 2002 *Proceedings of the Combustion Institute* **29** 2105–2111
- [72] Pitsch H and de Lageneste L D 2002 *Proceedings of the Combustion Institute* **29** 2001–2008
- [73] Hawkes E R and Cant R S 2000 *Proceedings of the Combustion Institute* **28** 51–58
- [74] Hawkes E R and Cant R S 2001 *Combustion Theory and Modelling* **5** 699–720
- [75] Colin O, Ducros F, Veynante D and Poinot T 2000 *Physics of Fluids* **12** 1843–1863
- [76] Chakravarthy V K and Menon S 2001 *Combustion Science and Technology* **162** 175–222
- [77] Sankaran V and Menon S 2005 *Proceedings of the Combustion Institute* **30** 575–582
- [78] Pantano C and Sarkar S 2001 *Physics of Fluids* **13** 3803–3819
- [79] Mellado J P, Sarkar S and Pantano C 2003 *Physics of Fluids* **15** 3280–3307
- [80] Kaiser S A and Frank J H 2007 *Proceedings of the Combustion Institute* **31** 1515–1523
- [81] Frank J H and Kaiser S A 2008 *Experiments in Fluids* **44** 221–233 doi 10.1007/s00348-007-0396-x
- [82] Pickett L M 2005-2011 Engine combustion network [www.ca.sandia.gov/ECN](http://www.ca.sandia.gov/ECN) Combustion Research Facility, Sandia National Laboratories
- [83] Oefelein J C and Lacaze G 2011 *Proceedings of the 23rd International Colloquium on the Dynamics of Explosions and Reactive Systems* Irvine, California
- [84] Dahms R N, Pickett L M and Oefelein J C 2011 *Proceedings of the 23rd Annual Conference on Liquid Atomization and*

*Spray Systems* Ventura, California  
[85] Najm H N 2009 *Annual Review of Fluid Mechanics* **41** 35–52 dOI 10.1146/annurev.fluid.010908.165248